symmetry

IMPACT FACTOR 2.940

CITESCORE 4.3

Article

Stellar β^- Decay Rates for ^{63}Co and ^{63}Ni by the Projected Shell Model

Zi-Rui Chen and Long-Jun Wang

Special Issue

Symmetry in Nuclear Physics: Model Calculations, Advances and Applications

Edited by

Prof. Dr. Jerry Paul Draayer, Dr. Feng Pan and Dr. Andriana Martinou

MDPI

https://doi.org/10.3390/sym15020315

symmetry

MDPI

Article

Stellar β^- Decay Rates for ^{63}Co and ^{63}Ni by the Projected Shell Model

Zi-Rui Chen and Long-Jun Wang *

School of Physical Science and Technology, Southwest University, Chongqing 400715, China
* Correspondence: longjun@swu.edu.cn

Abstract: β^- decay for ^{63}Co-^{63}Ni-^{63}Cu region nuclei play important roles in core-collapse supernovae and the slow neutron-capture (*s*) process. In this work, the stellar β^- decay rates for ^{63}Co and ^{63}Ni are studied within the projected shell model where the effects of thermally populated parent-nucleus excited states are analyzed. For ^{63}Co, the calculated stellar β^- decay rates are lower than the results of the conventional shell model. For the *s*-process branching point ^{63}Ni, the β^- decay rate under a terrestrial condition is well described, and the calculated stellar β^- decay rates in the *s*-process condition turn out to increase with stellar temperature due to the contribution from parent-nucleus excited states.

Keywords: β^- decay; *s*-process; branching point; core-collapse supernova; projected shell model

check for updates

Citation: Chen, Z.-R.; Wang, L.-J. Stellar β^- Decay Rates for ^{63}Co and ^{63}Ni by the Projected Shell Model. *Symmetry* **2023**, *15*, 315. https://doi.org/10.3390/sym15020315

Academic Editors: Jerry Paul Draayer, Feng Pan and Andriana Martinou

Received: 26 December 2022
Revised: 14 January 2023
Accepted: 17 January 2023
Published: 22 January 2023

1. Introduction

Weak interaction processes of finite nuclei play crucial roles in many frontiers in particle physics, nuclear physics and nuclear astrophysics. The neutrinoless double β decay is expected to help us understand the nature of neutrinos and new physics beyond the standard model [1–3]. β spectrum and anti-neutrino spectrum of nuclear single β decay are critical for the determination of safety procedures for nuclear power plant operation [4]. More importantly, the understanding of astrophysical problems such as the evolution of stars, the origin of heavy elements etc. rely heavily on reliable weak-interaction process rates of finite nuclei in stellar environments with high temperature and high density [5–9].

Stellar weak-interaction processes of finite nuclei mainly include nuclear β^- decay, β^+ decay, electron capture and positron capture processes in stellar environments. They can lead to three kinds of effects, changing protons into neutrons or vice versa, reducing the number of electrons or positrons in the environment, and emitting neutrinos which can escape the environment unhindered in most cases [5–11]. The nuclear stellar weak-interaction processes' rates then turn out to be crucial inputs for understanding the core-collapse supernova of massive stars [12], the slow neutron-capture (*s*) process [13], the rapid neutron-capture (*r*) process [14], the rapid proton-capture (*rp*) process [15], the cooling of neutron stars, etc. [16,17].

It is expected generally that the allowed Gamow–Teller (GT) transition should give a dominant contribution to stellar weak-interaction process rates [18], although the first forbidden transitions would probably be non-negligible in many cases [19], especially for heavy neutron-rich nuclei with large deformation. The reduced GT transition strength function $B(\mathrm{GT})$ then plays crucial roles in deriving (calculating) stellar weak-interaction process rates. Experimentally, the $B(\mathrm{GT})$ distributions can be measured by either the traditional β-decay experiments or the modern charge-exchange (CE) reactions, for nuclei near or not far from the β stability valley, under terrestrial conditions, i.e., when the parent nuclei always stay in their ground states (g.s.) [20–24]. However, on one hand, a large number of nuclei far from the β stability valley are involved and then important for many astrophysical problems such as the *r*-process, *rp*-process, cooling of neutron stars, etc. On

the other hand, in stellar environments with high temperature and high density, nuclei can have considerable probability to be thermally populated in their excited states. Systematical studies for $B(\mathrm{GT})$ distributions of nuclei far from the β stability valley and/or from excited states of parent nuclei are still beyond the capacity of current experimental techniques. Therefore, theoretical calculations are relied on heavily currently and in the near future.

Theoretically, over the past few decades, many nuclear structure models have been developed to study the $B(\mathrm{GT})$ distributions and stellar weak-interaction process rates. The pioneering work for systematical estimation of nuclear stellar weak-interaction process rates was completed by Fuller, Fowler and Newman (FFN) [5–8]. In modern treatments, the conventional shell model (SM), with a full diagonalization of an effective Hamiltonian in a chosen model space, is regarded as the most reliable method for GT transition and stellar weak-interaction process rates calculations [9,22]. This method is successfully applied to calculate nuclear weak-interaction processes in sd-shell [10,25,26] and pf-shell [27,28] (up to the mass-60 region) nuclei. While considering heavier and deformed nuclei, the SM is inhibited due to the inevitable explosion of large model- and configuration-space dimensions in numerical calculations. Other approaches are expected in applications for the $B(\mathrm{GT})$ distributions and stellar weak-interaction process rates, such as the hybrid model based on the shell model Monte Carlo approach and the random-phase approximation [29,30], and the quasiparticle random-phase approximation (QRPA) with different energy density functionals [31–40], by which nuclei in the whole nuclear landscape can be touched. Recently, the traditional Projected Shell Model (PSM) [41,42] has been developed for studying GT transitions as well [43,44]; in particular, the configuration space is extended for calculating $B(\mathrm{GT})$ distributions by Wang and collaborators [44]. This new method has been applied successfully in stellar weak-interaction rates calculations, such as the stellar electron capture process [45–47], the Urca cooling of neutron stars [17], etc. Some important algorithms for angular-momentum projection are also proposed [48–54].

Massive stars end their lives by core-collapse supernova explosion, leaving neutron stars or black holes as remnants. Before supernova, massive stars have onion-like structure, where the Fe-Co-Ni mass-region nuclei play important roles in the core. Before the core collapse, nuclear β decays compete with electron captures depending on neutron excess [55,56], determining the electron degeneracy pressure. ^{63}Co is one of the most important β-decaying nuclei in a presupernova collapse [18]. On the other hand, most heavy elements (nuclei) near or in the β stability valley are expected to be synthesized originally by the s process where the neutron-capture time scale is slower than that for β decay [13]. One of the crucial topics for s-process study is the s-process branching (or branch-point nucleus) for which the neutron capture and β decay have a similar time scale approximately and compete with each other, affecting the s-process abundance distribution or local abundance ratio [13]. ^{63}Ni is one of the s-process branchings, and the corresponding β decay rates under stellar conditions are then much desired.

In this work, we perform PSM calculations for stellar β^- decay rates for the first time by taking β^- decay from ^{63}Co to ^{63}Ni in a presupernova-collapse condition with high density and high temperature and β^- decay from ^{63}Ni to ^{63}Cu in the s-process conditions as first examples. The paper is organized as follows. In Section 2, we briefly introduce the formalism for calculation of β^- decay rates in astrophysical environments based on the PSM. In Section 3, we provide level schemes of ^{63}Co, ^{63}Ni, and ^{63}Cu, as well as their stellar β^- decay rates. Finally, we summarized our work in Section 4.

2. Theoretical Framework

Although nuclear isomers are expected to play crucial roles in stellar weak-interaction processes in some cases [57], here, we follow the assumption that parent nuclei are in a

thermal equilibrium with occupation probability for excited states following the Boltzmann distribution. Following the FFN work [5–8], stellar β^- decay rates read as,

$$\lambda^{\beta^-} = \frac{\ln 2}{K} \sum_i \frac{(2J_i+1)e^{-E_i/(k_B T)}}{G(Z,A,T)} \sum_f B_{if} \Phi_{if}^{\beta^-}, \tag{1}$$

where the constant K can be determined from the superallowed Fermi transition and $K = 6146 \pm 6\ s$ [58] is adopted in this work. The summations in Equation (1) run over initial (i) and final (f) states of parent and daughter nuclei, respectively (with angular momenta J_i, J_f and excitation energies E_i, E_f). k_B represents the Boltzmann constant while T is the environment temperature. $G(Z,A,T) = \sum_i (2J_i+1)\exp(-E_i/(k_B T))$ is the partition function of the parent nuclei. $\Phi_{if}^{\beta^-}$ is the phase space integral given as,

$$\Phi_{if}^{\beta^-} = \int_1^{Q_{if}} \omega p (Q_{if}-\omega)^2 F(Z+1,\omega)(1-S_e(\omega))(1-S_\nu(Q_{if}-\omega))d\omega \tag{2}$$

where ω and $p = \sqrt{\omega^2-1}$ label the total energy (rest mass and kinetic energy) and the momentum of the electron in units of $m_e c^2$ and $m_e c$, respectively. The available total energy of a one-to-one β^- transition is given by,

$$Q_{if} = \frac{1}{m_e c^2}(M_p - M_d + E_i - E_f) \tag{3}$$

where $M_p(M_d)$ indicates the nuclear mass of parent (daughter) nucleus. In Equation (2), S_e is the electron distribution function following the Fermi–Dirac distribution as,

$$S_e(\omega) = \frac{1}{\exp[(\omega-\mu_e)/k_B T]+1} \tag{4}$$

in which the chemical potential, μ_e, is determined from the relation,

$$\rho Y_e = \frac{1}{\pi^2 N_A}\left(\frac{m_e c}{\hbar}\right)^3 \int_0^\infty (S_e - S_p) p^2 dp \tag{5}$$

here, N_A represents Avogadro's number, and ρY_e represents the electron density. Note that one can obtain the positron distribution S_p by the replacement $\mu_p = -\mu_e$. The (anti-)neutrino distribution function S_ν in Equation (2) is adopted as $S_\nu = 0$ as usual [18]. The Fermi function $F(Z+1,\omega)$ in Equation (2) that reveals the distribution of the electron wave function near the nucleus can be found in Refs. [5,18] with Z being the proton number of the decaying (parent) nucleus.

The last part of Equation (1), B_{if}, is the reduced transition probability of the one-to-one nuclear β^- transition. In the present work, we only consider GT contributions, following Refs. [22,38],

$$B_{if} = B(\mathrm{GT}^-)_{if} = \left(\frac{g_A}{g_V}\right)^2_{\mathrm{eff}} \frac{\left\langle \Psi_{J_f}^{n_f} \middle\| \sum_k \hat{\sigma}^k \hat{\tau}_-^k \middle\| \Psi_{J_i}^{n_i} \right\rangle^2}{2J_i+1}, \tag{6}$$

where the matrix element is reduced with respect to the Pauli spin operator $\hat{\sigma}$, while $\hat{\tau}_-$ is the isospin lowering operator which changes a neutron into a proton as for β^- decay and the sum run over all nucleons. The nuclear many-body wave function, Ψ_J^n, represents the n-th eigen-state for angular momentum J and the index i (f) is for the parent (daughter) nucleus. $(g_A/g_V)_{\mathrm{eff}}$ is the effective ratio of axial and vector coupling constants with corresponding quenching of the GT strength [59,60]

$$\left(\frac{g_A}{g_V}\right)_{\mathrm{eff}} = f_{\mathrm{quench}} \left(\frac{g_A}{g_V}\right)_{\mathrm{bare}} \tag{7}$$

where $(g_A/g_V)_{\text{bare}} = -1.2599(25)$ [58] or $= -1.27641(45)$ [61], and f_{quench} is the quenching factor for which $f_{\text{quench}} = 0.75$ is adopted in this work.

From Equation (1) to Equation (7), as the electron chemical potential can be determined with given stellar temperature and electron density by Equation (5), it is seen that the only important part that one needs to consider so far is the reduced probability of nuclear transitions. The calculation of $B(\text{GT}^-)_{if}$ in Equation (6) is not easy, for which the nuclear many-body wave functions in the laboratory frame with good angular momentum and parity should be prepared as the GT operator has a strong selection rule. In the present work, we follow Refs. [17,44–46] and apply the PSM method to calculate GT transition strengths among odd-mass nuclei.

Different from the conventional shell model which constructs the configurations in a large spherical harmonic basis, the projected shell model begins with the deformed Nilsson single particle basis [62], with pairing correlations incorporated [41] into the basis by a BCS calculation for the Nilsson states. Therefore, the Nilsson–BCS calculation defines a deformed quasiparticle (qp) basis and describes nuclei in the intrinsic frame. Such a picture provides an efficient way to avoid the problem of dimension explosion while treating the heavier shells, as different-order of qp configurations in large model space can be constructed with a clearly physical pattern for dimension truncations. For odd-neutron nuclei, the configurations in PSM are written as,

$$\begin{aligned}&\{\hat{a}^\dagger_{\nu_i}|\phi(\varepsilon)\rangle,\ \hat{a}^\dagger_{\nu_i}\hat{a}^\dagger_{\nu_j}\hat{a}^\dagger_{\nu_k}|\phi(\varepsilon)\rangle,\ \hat{a}^\dagger_{\nu_i}\hat{a}^\dagger_{\pi_j}\hat{a}^\dagger_{\pi_k}|\phi(\varepsilon)\rangle\\&\hat{a}^\dagger_{\nu_i}\hat{a}^\dagger_{\nu_j}\hat{a}^\dagger_{\nu_k}\hat{a}^\dagger_{\pi_l}\hat{a}^\dagger_{\pi_m}|\phi(\varepsilon)\rangle\ldots\}\end{aligned} \tag{8}$$

and for odd-proton nuclei,

$$\begin{aligned}&\{\hat{a}^\dagger_{\pi_i}|\phi(\varepsilon)\rangle,\ \hat{a}^\dagger_{\pi_i}\hat{a}^\dagger_{\pi_j}\hat{a}^\dagger_{\pi_k}|\phi(\varepsilon)\rangle,\ \hat{a}^\dagger_{\pi_i}\hat{a}^\dagger_{\nu_j}\hat{a}^\dagger_{\nu_k}|\phi(\varepsilon)\rangle\\&\hat{a}^\dagger_{\pi_i}\hat{a}^\dagger_{\pi_j}\hat{a}^\dagger_{\pi_k}\hat{a}^\dagger_{\nu_l}\hat{a}^\dagger_{\nu_m}|\phi(\varepsilon)\rangle\ldots\}\end{aligned} \tag{9}$$

where $|\phi(\varepsilon)\rangle$ labels the qp vacuum associated with the intrinsic deformation ε, and $\hat{a}^\dagger_\nu(\hat{a}^\dagger_\pi)$ labels the neutron (proton) qp creation operator. In this work, we choose four spherical harmonic oscillator major shells $(N = 2, 3, 4, 5)$ to establish the model space for calculating the β^- decay process for ^{63}Co-^{63}Ni-^{63}Cu.

The symmetries that are broken in the intrinsic frame can be restored by exact projection techniques [63]. The angular momentum (and if necessary, also particle number and parity) projection is performed on the qp basis to form a many-body basis in the laboratory frame. The angular momentum projection operator is written as,

$$\hat{P}^J_{MK} = \frac{2J+1}{8\pi^2}\int d\Omega D^J_{MK}(\Omega)\hat{R}(\Omega) \tag{10}$$

where $\hat{R}$ and D^J_{MK} (with Euler angle Ω [64]) are the rotation operator and Wingner D-function, respectively. The nuclear many-body wave function in the laboratory frame can then be expressed as,

$$|\Psi^n_{JM}\rangle = \sum_{K\kappa} F^n_{JK\kappa}\hat{P}^J_{MK}|\phi_\kappa(\varepsilon)\rangle \tag{11}$$

where $|\phi_\kappa(\varepsilon)\rangle$ represents the qp configurations given in Equations (8) and (9). The expansion coefficients $F^n_{JK\kappa}$ can be obtained by solving the Hill–Wheeler–Griffin equation in PSM, where a separable two-body GT force is included explicitly in the original PSM Hamiltonian (the details of the PSM for GT transition can be found in Ref. [44]).

3. Results and Discussions

3.1. Level Scheme

In Figure 1, we show the calculated energy level for the three nuclei (^{63}Co with $Z = 27$, $N = 36$, ^{63}Ni with $Z = 28$, $N = 35$, and ^{63}Cu with $Z = 29$, $N = 34$) and compared it with available data on the NNDC website [65]. The intrinsic quadrupole and hexadecapole deformation (ε_2 and ε_4) in Equations (8) and (9) are adopted following Ref. [66] from which $\varepsilon_2 \approx 0.12$ for the three involved nuclei. It is seen from Figure 1 that for both ^{63}Co and ^{63}Cu, the ground states are well reproduced with reasonable angular momentum and parity. The gap between the ground states and the first excited states for ^{63}Co and ^{63}Cu is well described, indicating that the $Z = 28$ shell gap originating from the $\pi f_{7/2}$ orbital is reproduced reasonably. For ^{63}Ni, the neutron Fermi surface locates in a high single-particle level density region caused by the $\nu p_{3/2}, f_{5/2}, p_{1/2}$ orbitals. Some low-lying states are found experimentally to be near the ground state within about 200 keV excitation energy. The calculations reproduce these low-lying states while giving inapposite angular momentum and parity for the ground states. For the ground state and low-lying states of ^{63}Ni, it is noted that the calculations by the conventional shell model with the jj44b interaction give the same results as our PSM, the calculations with the JUN45 interaction can reproduce the angular momentum and parity of the ground state, while the calculated excitation energies for low-lying states are much higher than the data [67].

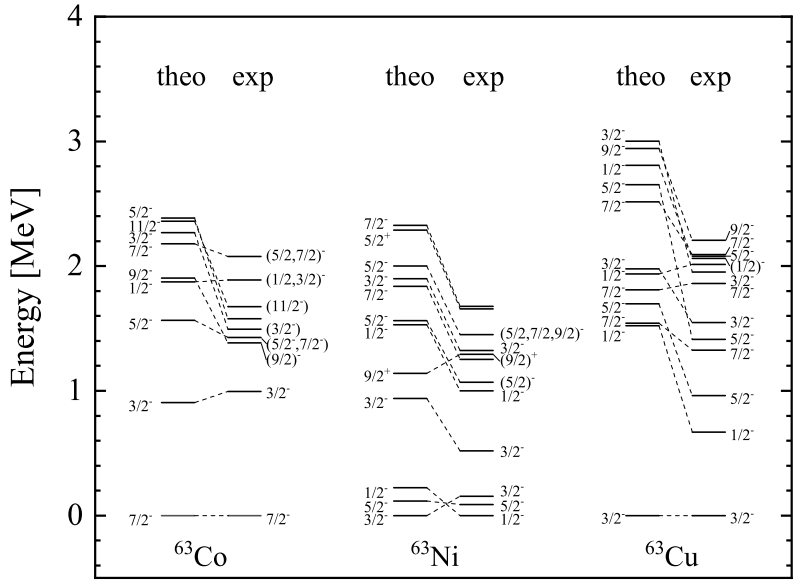

Figure 1. Calculated energy levels for ^{63}Co-^{63}Ni-^{63}Cu as compared with experimental data [65].

As will be seen later, the ground states and low-lying states of parent nuclei play important roles in stellar β-decay rates calculations. Here, we represent the detailed configuration information of corresponding wave functions for the three involved nuclei; only the main configurations are mentioned as strong configuration mixing exists in most wave functions. For the ground state of ^{63}Co, it is described as 38% $\pi 7/2^-[303]$ with 27% $\pi 5/2^-[312]$ (the Nilsson notation [62]) originating from the $\pi f_{7/2}$ orbital as well as the strong mixing of many 3qp configurations. For ^{63}Ni, the ground state and two low-lying states with $J^\pi = 3/2^-, 5/2^-$, and $1/2^-$ are mainly constructed by 66% $\nu 3/2^-[312]$ with 17% $\nu 1/2^-[321]$, 31% $\nu 1/2^-[310]$ and 31% $\nu 3/2^-[301]$ with 27% $\nu 5/2^-[303]$, and 28% $\nu 1/2^-[310]$ with 50% $\nu 1/2^-[301]$ respectively, originating from the $\nu p_{1/2}, f_{5/2}, p_{3/2}$ orbitals, and mixing with 3qp configurations. The ground state of ^{63}Cu is described by 18% $\pi\, 1/2^-[321]$ with 44% $\pi\, 3/2^-[312]$ ($p_{3/2}$ orbital).

3.2. β^- Decay from ^{63}Co to ^{63}Ni

The core collapse of a massive star happens usually with much high temperature and density, and ^{63}Co is one of the most important β-decaying nuclei in a presupernova collapse [18]. Thus, here, we study the stellar β^- decay rates of ^{63}Co for a stellar temperature range between 1 and 10 GK with different electron densities ρY_e ($10^7, 10^8, 10^9$, and 10^{10}, in mol/cm^3).

In Figure 2a,b, we first show the calculated $B(\mathrm{GT}^-)$ distribution (blue) from the ground state ($J^\pi = 7/2^-$) and the first excited state ($J^\pi = 3/2^-$) of ^{63}Co to all related states of ^{63}Ni below $Q_\beta = 3672$ keV as a function of the excitation energy for the daughter nucleus E_x, respectively, and compared them with available experimental data (red) [65]. It can be seen from Figure 2a that the $B(\mathrm{GT}^-)$ from the ground state of the parent to the daughter nucleus was described well compared with the data. The $B(\mathrm{GT}^-) \approx 0.1$ from the ground state of ^{63}Co to the low-lying $5/2^-$ state of ^{63}Ni at $E_x \approx 100$ keV is well reproduced. The $B(\mathrm{GT}^-)$ values from ground state to states with higher E_x is also described reasonably, where a shift of E_x toward higher excitation energy is found. This is caused by the fact that the calculated $5/2^-, 7/2^-, 9/2^-$ states of ^{63}Ni by our PSM are about 0.5 MeV higher than the corresponding experimental levels, as can be seen from Figure 1.

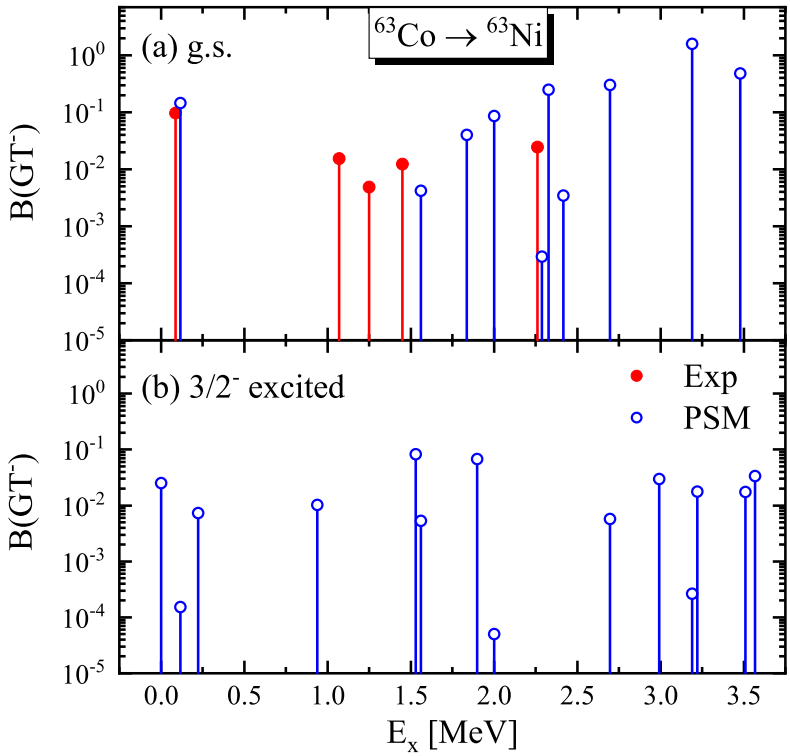

Figure 2. The calculated (blue) and experimental (red) [65] $B(\mathrm{GT}^-)$ distribution from the ground state (g.s., as in panel (**a**)) of ^{63}Co, as well as from the first excited state ($J^\pi = 3/2^-$, as in panel (**b**)) of ^{63}Co, to all related states of ^{63}Ni below the Q value $Q_{\beta^-} = 3672$ keV [65].

In Figure 2b, it can be seen that with the first excited state of ^{63}Co with $J^\pi = 3/2^-$, the low-lying $1/2^-, 3/2^-$ states of ^{63}Ni can now be connected by GT transitions. The predicted two $B(\mathrm{GT}^-)$ values are about 0.02, while the predicted $B(\mathrm{GT}^-)$ value to the low-lying $5/2^-$ is as small as about 10^{-4}, which is much smaller than the case of the ground state of ^{63}Co. In addition, $B(\mathrm{GT}^-)$ distribution from the excited state is more diffuse than the case of the ground state, as shown in Figure 2a. These results may affect the corresponding stellar β^- rates at higher temperature when the excited states of parent nuclei can be thermally populated and contribute to the stellar β^- rates.

Figure 3 shows the calculated stellar β^- decay rates from ^{63}Co to ^{63}Ni at different temperature and densities, which are compared with the corresponding calculations from

the conventional shell model by Langanke and Martínez-Pinedo (LMP) [18]. It should be noted that in the latter calculations, experimental data for energies and GT strengths are adopted whenever available (see Ref. [18] for details). For comparison, available data for energies and GT strengths are adopted in the calculations by the PSM as well. For large density $\rho Y_e = 10^{10}$ mol/cm^3, the electron chemical potential μ_e is as high as about 10 MeV, so that only transitions to the ground state or relatively low-lying states of ^{63}Ni can contribute to the stellar β^- decay rates. In this case, at low temperature T_9, the parent nucleus ^{63}Co stays basically in its ground state, and the resulting β^- decay rates are negligible as seen from Figure 3d, owing to the fact that the ground-state-to-ground-state transition is forbidden. With increasing temperature, the transitions among excited states of parent and daughter nuclei begin to contribute, and the resulting β^- decay rates are found to increase rapidly with T_9. Our calculations give very similar β^- decay rates as the LMP results at low temperature, as seen from Figure 3d, as both methods adopted available data. While for cases of high temperature, when many excited states of the parent nucleus contribute, the PSM results are found to be smaller than the LMP results.

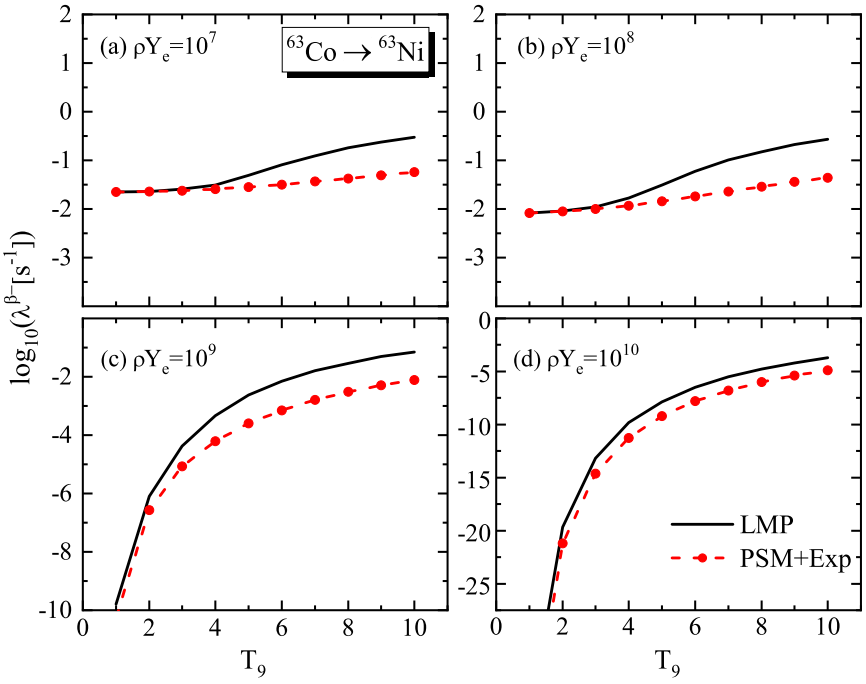

Figure 3. The stellar β^--decay rates from ^{63}Co to ^{63}Ni as a function of the stellar temperature T_9 (in GK) for densities $\rho Y_e = 10^7, 10^8, 10^9$, and 10^{10} mol/cm^3. Calculations by the PSM with available data adopted (red dashed with symbols) are shown and compared with the results from the conventional shell model [18] (black solid).

When the density decreases, for $\rho Y_e = 10^7, 10^8, 10^9$ mol/cm^3, the μ_e decreases as well ($\mu_e \approx 1.2$ MeV for $\rho Y_e = 10^7$ mol/cm^3). In these cases, GT transitions to many excited states of the daughter nucleus would contribute to the stellar β^- decay rates as well, and the corresponding β^- decay rates increase with decreasing ρY_e, as seen from Figure 3a–c. The PSM calculations provide smaller β^- decay rates than the shell-model results of LMP by about one order of magnitude at high temperature when the thermal population of excited states of the parent nucleus is possible. This indicates that the $B(\mathrm{GT}^-)$ values from the $3/2^-$ and many other excited state of ^{63}Co from PSM calculations should be smaller than those of shell-model calculations of LMP. As ^{63}Co is one of the most important β-decaying nuclei in a presupernova collapse [18], a systematical study of stellar β^- decay rates in this mass region is planned as future works for understanding the possible effects of our PSM calculations on core-collapse supernova.

3.3. β^- Decay from ^{63}Ni to ^{63}Cu

As one of the branch-point nuclei in the *s* process, reliable stellar β^- decay rates and the neutron capture cross-section for ^{63}Ni are much desired [68]. Depending on the neutron density and temperature of the *s* process, ^{63}Ni can either β^- decay to ^{63}Cu or capture neutrons to synthesize ^{64}Ni. Reliable stellar β^- decay rates of ^{63}Ni are then crucial for understanding of the branching ratio, the abundances of Cu isotopes, etc. Here, we focus on β^- decay rates calculations in *s*-process environments with temperature range from 0.1 to 1 GK. Since the Q value for β^- decay of ^{63}Ni is as small as 67 keV, we show in Figure 4 the decay scheme instead of the GT strength distributions. In Figure 4, the excitation energies (keV), J^π, logft values, and Q_{β^-} values are taken from Ref. [65]. We supplement data with theoretical logft values (in parentheses) calculated from PSM. Under terrestrial condition, the parent nucleus ^{63}Ni stays in its ground state with $J^\pi = 1/2^-$, which can only decay to the ground state of the daughter nucleus ^{63}Cu due to the small Q_{β^-} value. The corresponding logft value was measured to be 6.70, which is described reasonably by our PSM calculations, which give logft = 6.36.

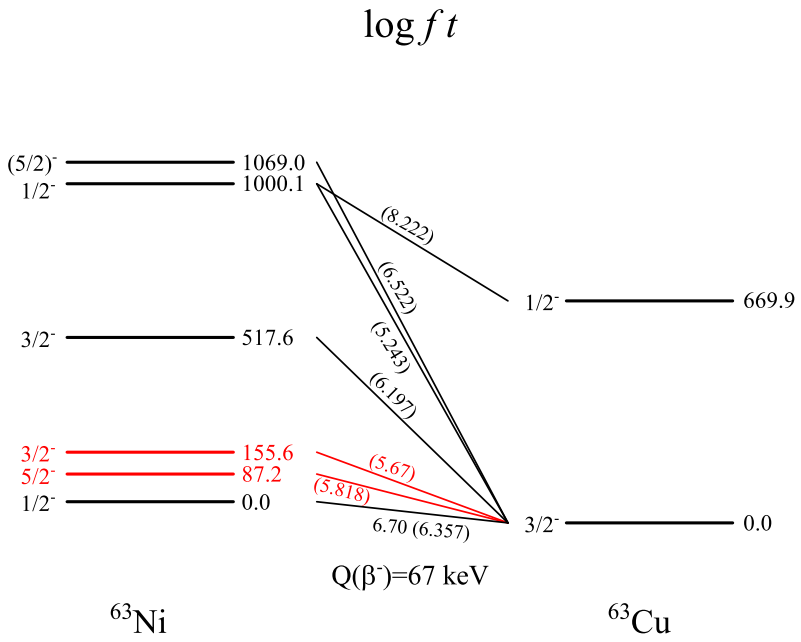

Figure 4. The decay scheme for β^- decay from ^{63}Ni and ^{63}Cu that is crucial in the stellar environment. Nuclear low-lying states for both parent and daughter nuclei and individual transitions between them are shown, where the angular–momentum–parity assignment J^π, excitation energy (in keV), Q-value (in keV) and logft for allowed GT transition are taken from the data [65] when available and supplemented by PSM calculations (in parenthesis for logft). The levels and transitions displayed in red play crucial roles in stellar environments.

In *s*-process environments, the stellar temperature can be as high as 1 GK and beyond so that the two low-lying states of ^{63}Ni (with excitation energy 87.2 keV and 155.6 keV, respectively, see Figure 4) can be easily populated thermally with large probabilities. Transitions from these low-lying states can hardly be touched experimentally so far, and the corresponding logft values are predicted by our PSM calculations to be about 5.7, as displayed in red in Figure 4, which is much stronger than the transition from the ^{63}Ni ground state. This should be caused by the different configuration mixing in wave functions of the low-lying and ground states, as discussed in the context of Figure 1. In the following, we study the effect of such thermal population of low-lying states on the stellar β^- decay rates.

With the nuclear properties shown in Figure 4, a full calculation for the stellar β^- decay rates for the ^{63}Ni $\rightarrow$ ^{63}Cu case in *s*-process environments (with temperature from 1 to 10 in 10^8 K, electron density ρY_e from 10^2 to 10^5 in mol/cm^3) can be performed by Equation (1). The corresponding results are plotted in Figure 5 where the first ten levels with excitation energies less than 1.451 MeV are considered in calculations. To illustrate the effects of excited states of the parent nucleus, we also compare these full calculations with the unrealistic cases where only ground-state-to-ground-state transition is considered (i.e., setting $B(\mathrm{GT}^-)_{if} = 0$ unless for $i = f = 1$ in Equation (1)). These unrealistic results are also shown in Figure 5 (labeled by 'g.s.') for comparison. The electron chemical potential μ_e is similar in the four electron density cases ($\mu_e \approx 0.5$ MeV), which is larger than the Q_{β^-} value. Therefore, the transition between ground states contributes mainly to the decay rates at low temperature. With the increase of temperature, the stellar population probability of the ^{63}Ni ground state decreases, leading to decreasing unrealistic decay rates with the temperature, as seen from the lines with symbols in Figure 5.

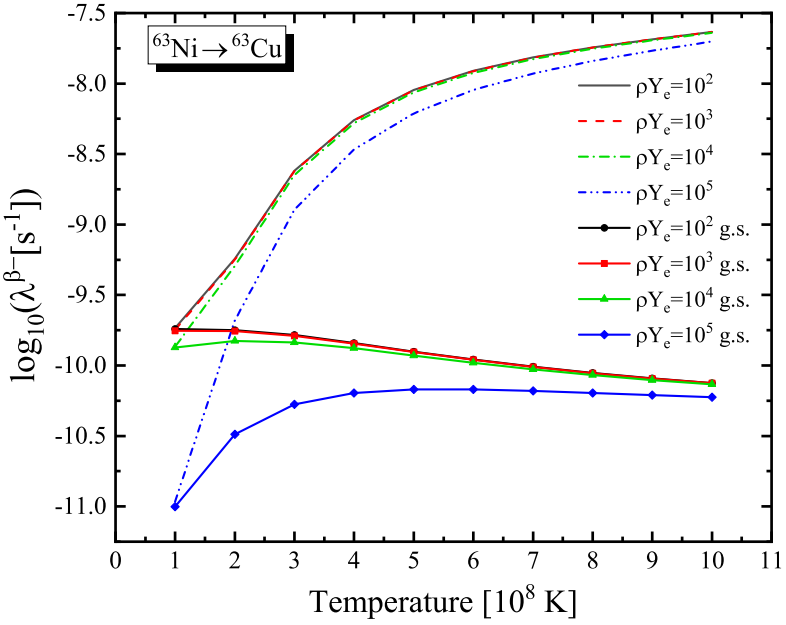

Figure 5. The calculated β^- decay rates for the ^{63}Ni $\rightarrow$ ^{63}Cu case in stellar environments with different density ρY_e (in mol/cm^3) and temperature (in 10^8 K). Calculations with (realistic) and without (unrealistic, with symbols) the contributions of excited parent-nucleus states are shown for comparison.

When contributions from the low-lying states of the parent nucleus ^{63}Ni (see levels in red in Figure 4) to the decay rates are taken into account in the full calculations, as the stellar population probabilities of the low-lying states increase with the temperature, on one hand, the practical Q_{if} values increase dramatically from 67 keV to $67 + 87.2 = 154.2$ keV and $67 + 155.6 = 222.6$ keV; on the other hand, the GT transitions from low-lying states are predicted to be about one order of magnitude stronger than the transition between ground states, as can be seen in Figure 4. Both mechanisms tend to increase the corresponding stellar β^- decay rates, and the resulting decay rates at 1 GK temperature and beyond turn out to be more than two orders of magnitude larger than the one under terrestrial condition.

4. Summary

To summarize, stellar β^- decay rates are crucial nuclear inputs for understanding many astrophysical processes, such as the core-collapse supernovae, the origin of elements heavier than iron by the *s*, *r* and *rp* processes, etc. In stellar environments with high temperature and density, parent nuclei have large probabilities to be thermally populated in their excited states, which would enhance significantly the corresponding stellar β^-

decay rates accordingly. In this work, we focus on the stellar β^- decay rates of nickel region nuclei by taking ^{63}Co, ^{63}Ni, and ^{63}Cu as examples. Following the FFN formalism with the assumption of thermal equilibrium as well as applying the projected shell model for the description of nuclear many-body wave functions and GT transitions, the stellar β^- decay rates of ^{63}Co and ^{63}Ni are calculated and analyzed. For β^- decay from ^{63}Co to ^{63}Ni, which is important in a presupernova collapse, we found that the decay rates are sensitive to stellar temperature at higher electron densities but not obviously dependent on the temperature at relatively lower densities. When compared with the results of a conventional shell model by LMP, our calculations give lower decay rates within one order of magnitude. For the *s*-process branching ^{63}Ni, to discuss the effects of excited nuclear states, we calculate the β^- decay rates in different cases and compare them with the unrealistic one in which only ground-state-to-ground-state transition is considered. It is found that in the *s*-process, the decay rates enhance dramatically when contributions from excited parent-nucleus states are taken into account, which increase by more than two orders of magnitude at 1 GK temperature and beyond.

The effects of the thermally populated excited states of parent nuclei on corresponding stellar weak-interaction process rates depend on detailed nuclear structure and are a crucial topic for many astrophysical phenomena. The topic is worth studying by many nuclear-structure approaches, and systematic research by our projected shell model is planned as future works.

Author Contributions: Conceptualization, Z.-R.C. and L.-J.W.; methodology, L.-J.W.; software, L.-J.W.; investigation, Z.-R.C.; data curation, Z.-R.C.; writing—original draft preparation, Z.-R.C. and L.-J.W.; writing—review and editing, L.-J.W. All authors have read and agreed to the published version of the manuscript.

Funding: This work is supported by the National Natural Science Foundation of China (Grants No. 12275225), by the Fundamental Research Funds for the Central Universities (Grant No. SWU-KT22050), and partially supported by the Key Laboratory of Nuclear Data (China Institute of Atomic Energy).

Institutional Review Board Statement: Not applicable.

Informed Consent Statement: Not applicable.

Data Availability Statement: Not applicable.

Acknowledgments: L.J.W. would like to thank F. Pan and B. H. Sun for invitation and discussions.

Conflicts of Interest: The authors declare no conflict of interest.

References

1. Avignone, F.T.; Elliott, S.R.; Engel, J. Double beta decay, Majorana neutrinos, and neutrino mass. *Rev. Mod. Phys.* **2008**, *80*, 481–516. [CrossRef]
2. Wang, L.J.; Engel, J.; Yao, J.M. Quenching of nuclear matrix elements for $0\nu\beta\beta$ decay by chiral two-body currents. *Phys. Rev. C* **2018**, *98*, 031301(R). [CrossRef]
3. Yao, J.M.; Engel, J.; Wang, L.J.; Jiao, C.F.; Hergert, H. Generator-coordinate reference states for spectra and $0\nu\beta\beta$ decay in the in-medium similarity renormalization group. *Phys. Rev. C* **2018**, *98*, 054311. [CrossRef]
4. Fijałkowska, A.; Karny, M.; Rykaczewski, K.P.; Rasco, B.C.; Grzywacz, R.; Gross, C.J.; Wolińska-Cichocka, M.; Goetz, K.C.; Stracener, D.W.; Bielewski, W.; et al. Impact of Modular Total Absorption Spectrometer measurements of β decay of fission products on the decay heat and reactor $\overline{\nu}_e$ flux calculation. *Phys. Rev. Lett.* **2017**, *119*, 052503. [CrossRef] [PubMed]
5. Fuller, G.M.; Fowler, W.A.; Newman, M.J. Stellar weak-interaction rates for sd-shell nuclei. I. Nuclear matrix element systematics with application to ^{26}Al and selected nuclei of imprtance to the supernova problem. *Astrophys. J. Suppl. Ser.* **1980**, *42*, 447–473. [CrossRef]
6. Fuller, G.M.; Fowler, W.A.; Newman, M.J. Stellar weak-interaction rates for intermediate-mass nuclei. II. *Astrophys. J.* **1982**, *252*, 715. [CrossRef]
7. Fuller, G.M.; Fowler, W.A.; Newman, M.J. Stellar weak-interaction rates for intermediate-mass nuclei. III. *Astrophys. J. Suppl. Ser.* **1982**, *48*, 279. [CrossRef]

8. Fuller, G.M.; Fowler, W.A.; Newman, M.J. Stellar weak-interaction rates for intermediate-mass nuclei. IV. *Astrophys. J.* **1985**, *293*, 1. [CrossRef]
9. Langanke, K.; Martínez-Pinedo, G. Nuclear weak-interaction processes in stars. *Rev. Mod. Phys.* **2003**, *75*, 819–862. [CrossRef]
10. Martínez-Pinedo, G.; Lam, Y.H.; Langanke, K.; Zegers, R.G.T.; Sullivan, C. Astrophysical weak-interaction rates for selected $A = 20$ and $A = 24$ nuclei. *Phys. Rev. C* **2014**, *89*, 045806. [CrossRef]
11. Langanke, K.; Martínez-Pinedo, G.; Zegers, R.G.T. Electron capture in stars. *Rep. Prog. Phys.* **2021**, *84*, 066301. [CrossRef] [PubMed]
12. Janka, H.T.; Langanke, K.; Marek, A.; Martínez-Pinedo, G.; Müller, B. Theory of core-collapse supernovae. *Phys. Rep.* **2007**, *442*, 38–74.
13. Käppeler, F.; Gallino, R.; Bisterzo, S.; Aoki, W. The *s* process: Nuclear physics, stellar models, and observations. *Rev. Mod. Phys.* **2011**, *83*, 157–193. [CrossRef]
14. Cowan, J.J.; Sneden, C.; Lawler, J.E.; Aprahamian, A.; Wiescher, M.; Langanke, K.; Martínez-Pinedo, G.; Thielemann, F.K. Origin of the heaviest elements: The rapid neutron-capture process. *Rev. Mod. Phys.* **2021**, *93*, 015002. . [CrossRef]
15. Schatz, H.; Aprahamian, A.; Görres, J.; Wiescher, M.; Rauscher, T.; Rembges, J.; Thielemann, F.K.; Pfeiffer, B.; Möller, P.; Kratz, K.L.; et al. rp-process nucleosynthesis at extreme temperature and density conditions. *Phys. Rep.* **1998**, *294*, 167–263. [CrossRef]
16. Schatz, H.; Gupta, S.; Möller, P.; Beard, M.; Brown, E.F.; Deibel, A.T.; Gasques, L.R.; Hix, W.R.; Keek, L.; Lau, R.; et al. Strong neutrino cooling by cycles of electron capture and β^- decay in neutron star crusts. *Nature* **2014**, *505*, 62. [CrossRef]
17. Wang, L.J.; Tan, L.; Li, Z.; Misch, G.W.; Sun, Y. Urca Cooling in Neutron Star Crusts and Oceans: Effects of Nuclear Excitations. *Phys. Rev. Lett.* **2021**, *127*, 172702. [CrossRef] [PubMed]
18. Langanke, K.; Martínez-Pinedo, G. Shell-model calculations of stellar weak interaction rates: II. Weak rates for nuclei in the mass range $A = 45 - 65$ in supernovae environments. *Nucl. Phys. A* **2000**, *673*, 481–508. [CrossRef]
19. Zhi, Q.; Caurier, E.; Cuenca-García, J.J.; Langanke, K.; Martínez-Pinedo, G.; Sieja, K. Shell-model half-lives including first-forbidden contributions for *r*-process waiting-point nuclei. *Phys. Rev. C* **2013**, *87*, 025803. [CrossRef]
20. Fujita, Y.; Rubio, B.; Gelletly, W. Spin–isospin excitations probed by strong, weak and electro-magnetic interactions. *Prog. Part. Nucl. Phys.* **2011**, *66*, 549–606. [CrossRef]
21. Zegers, R.G.T.; Akimune, H.; Austin, S.M.; Bazin, D.; Berg, A.M.d.; Berg, G.P.A.; Brown, B.A.; Brown, J.; Cole, A.L.; Daito, I.; et al. The (t,^{3}He) and (^{3}He, t) reactions as probes of Gamow-Teller strength. *Phys. Rev. C* **2006**, *74*, 024309. [CrossRef]
22. Cole, A.L.; Anderson, T.S.; Zegers, R.G.T.; Austin, S.M.; Brown, B.A.; Valdez, L.; Gupta, S.; Hitt, G.W.; Fawwaz, O. Gamow-Teller strengths and electron-capture rates for pf-shell nuclei of relevance for late stellar evolution. *Phys. Rev. C* **2012**, *86*, 015809. [CrossRef]
23. Misch, G.W.; Sprouse, T.M.; Mumpower, M.R.; Couture, A.J.; Fryer, C.L.; Meyer, B.S.; Sun, Y. Sensitivity of Neutron-Rich Nuclear Isomer Behavior to Uncertainties in Direct Transitions. *Symmetry* **2021**, *13*, 1831. [CrossRef]
24. Jian, H.; Gao, Y.; Dai, F.; Liu, J.; Xu, X.; Yuan, C.; Kaneko, K.; Sun, Y.; Liang, P.; Shi, G.; et al. β-Delayed γ Emissions of ^{26}P and Its Mirror Asymmetry. *Symmetry* **2021**, *13*, 2278. [CrossRef]
25. Oda, T.; Hino, M.; Muto, K.; Takahara, M.; Sato, K. Rate Tables for the Weak Processes of sd-Shell Nuclei in Stellar Matter. *At. Data Nucl. Data Tables* **1994**, *56*, 231. [CrossRef]
26. Misch, G.W.; Fuller, G.M.; Brown, B.A. Modification of the Brink-Axel hypothesis for high-temperature nuclear weak interactions. *Phys. Rev. C* **2014**, *90*, 065808. [CrossRef]
27. Caurier, E.; Langanke, K.; Martínez-Pinedo, G.; Nowacki, F. Shell-model calculations of stellar weak interaction rates. I. Gamow-Teller distributions and spectra of nuclei in the mass range A = 45–65. *Nucl. Phys. A* **1999**, *653*, 439. [CrossRef]
28. Langanke, K.; Martínez-Pinedo, G. Rate tables for the weak processes of pf-shell nuclei in stellar environments. *At. Data Nucl. Data Tables* **2001**, *79*, 1–46. [CrossRef]
29. Langanke, K.; Kolbe, E.; Dean, D.J. Unblocking of the Gamow-Teller strength in stellar electron capture on neutron-rich germanium isotopes. *Phys. Rev. C* **2001**, *63*, 032801(R). [CrossRef]
30. Langanke, K.; Martínez-Pinedo, G.; Sampaio, J.M.; Dean, D.J.; Hix, W.R.; Messer, O.E.B.; Mezzacappa, A.; Liebendörfer, M.; Janka, H.T.; Rampp, M. Electron Capture Rates on Nuclei and Implications for Stellar Core Collapse. *Phys. Rev. Lett.* **2003**, *90*, 241102. [CrossRef]
31. Engel, J.; Bender, M.; Dobaczewski, J.; Nazarewicz, W.; Surman, R. β decay rates of r-process waiting-point nuclei in a self-consistent approach. *Phys. Rev. C* **1999**, *60*, 014302. [CrossRef]
32. Paar, N.; Colò, G.; Khan, E.; Vretenar, D. Calculation of stellar electron-capture cross sections on nuclei based on microscopic Skyrme functionals. *Phys. Rev. C* **2009**, *80*, 055801. [CrossRef]
33. Bai, C.L.; Zhang, H.Q.; Sagawa, H.; Zhang, X.Z.; Colò, G.; Xu, F.R. Effect of the Tensor Force on the Charge Exchange Spin-Dipole Excitations of ^{208}Pb. *Phys. Rev. Lett.* **2010**, *105*, 072501. [CrossRef] [PubMed]
34. Dzhioev, A.A.; Vdovin, A.I.; Ponomarev, V.Y.; Wambach, J.; Langanke, K.; Martínez-Pinedo, G. Gamow-teller strength distributions at finite temperatures and electron capture in stellar environments. *Phys. Rev. C* **2010**, *81*, 015804. [CrossRef]
35. Niu, Y.F.; Niu, Z.M.; Colò, G.; Vigezzi, E. Particle-Vibration Coupling Effect on the β Decay of Magic Nuclei. *Phys. Rev. Lett.* **2015**, *114*, 142501. [CrossRef]

36. Fang, D.L.; Brown, B.A.; Suzuki, T. β decay properties for neutron-rich Kr-Tc isotopes from deformed pn-quasiparticle random-phase approximation calculations with realistic forces. *Phys. Rev. C* **2013**, *88*, 024314. [CrossRef]
37. Niu, Z.M.; Niu, Y.F.; Liang, H.Z.; Long, W.H.; Nikšić.; Vretenar, D.; Meng, J. β-decay half-lives of neutron-rich nuclei and matter flow in the r-process. *Phys. Lett. B* **2013**, *723*, 172. [CrossRef]
38. Sarriguren, P. Stellar electron-capture rates in p f-shell nuclei from quasiparticle random-phase approximation calculations. *Phys. Rev. C* **2013**, *87*, 045801. [CrossRef]
39. Robin, C.; Litvinova, E. Time-reversed particle-vibration loops and nuclear gamow-teller response. *Phys. Rev. Lett.* **2019**, *123*, 202501. [CrossRef]
40. Ejiri, H.; Suhonen, J.; Zuber, K. Neutrino–nuclear responses for astro-neutrinos, single beta decays and double beta decays. *Phys. Rep.* **2019**, *797*, 1. [CrossRef]
41. Hara, K.; Sun, Y. Projected shell model and high-spin spectroscopy. *Int. J. Mod. Phys. E* **1995**, *4*, 637–785. [CrossRef]
42. Sun, Y.; Feng, D.H. High spin spectroscopy with the projected shell model. *Phys. Rep.* **1996**, *264*, 375. [CrossRef]
43. Gao, Z.C.; Sun, Y.; Chen, Y.S. Shell model method for Gamow-Teller transitions in heavy, deformed nuclei. *Phys. Rev. C* **2006**, *74*, 054303. [CrossRef]
44. Wang, L.J.; Sun, Y.; Ghorui, S.K. Shell-model method for Gamow-Teller transitions in heavy deformed odd-mass nuclei. *Phys. Rev. C* **2018**, *97*, 044302. [CrossRef]
45. Tan, L.; Liu, Y.X.; Wang, L.J.; Li, Z.; Sun, Y. A novel method for stellar electron-capture rates of excited nuclear states. *Phys. Lett. B* **2020**, *805*, 135432. [CrossRef]
46. Wang, L.J.; Tan, L.; Li, Z.; Gao, B.; Sun, Y. Description of ^{93}Nb stellar electron-capture rates by the projected shell model. *Phys. Rev. C* **2021**, *104*, 064323. [CrossRef]
47. Lv, C.J.; Sun, Y.; Fujita, Y.; Fujita, H.; Wang, L.J.; Gao, Z.C. Effect of nuclear deformation on the observation of a low-energy super-Gamow-Teller state. *Phys. Rev. C* **2022**, *105*, 054308. [CrossRef]
48. Wang, L.J.; Chen, F.Q.; Mizusaki, T.; Oi, M.; Sun, Y. Toward extremes of angular momentum: Application of the Pfaffian algorithm in realistic calculations. *Phys. Rev. C* **2014**, *90*, 011303(R). [CrossRef]
49. Wang, L.J.; Sun, Y.; Mizusaki, T.; Oi, M.; Ghorui, S.K. Reduction of collectivity at very high spins in ^{134}Nd: Expanding the projected-shell-model basis up to 10-quasiparticle states. *Phys. Rev. C* **2016**, *93*, 034322. [CrossRef]
50. Wang, L.J.; Dong, J.; Chen, F.Q.; Sun, Y. Projected shell model analysis of structural evolution and chaoticity in fast-rotating nuclei. *J. Phys. G Nucl. Part. Phys.* **2019**, *46*, 105102. [CrossRef]
51. Wang, L.J.; Chen, F.Q.; Sun, Y. Basis-dependent measures and analysis uncertainties in nuclear chaoticity. *Phys. Lett. B* **2020**, *808*, 135676. [CrossRef]
52. Chen, Z.R.; Wang, L.J. Pfaffian formulation for matrix elements of three-body operators in multiple quasiparticle configurations. *Phys. Rev. C* **2022**, *105*, 034342. [CrossRef]
53. Wang, B.L.; Gao, F.; Wang, L.J.; Sun, Y. Effective and efficient algorithm for the Wigner rotation matrix at high angular momenta. *Phys. Rev. C* **2022**, *106*, 054320. [CrossRef]
54. Yokoyama, R.; Ideguchi, E.; Simpson, G.S.; Tanaka, M.; Sun, Y.; Lv, C.J.; Liu, Y.X.; Wang, L.J.; Nishimura, S.; Doornenbal, P.; et al. Three-quasiparticle isomers in odd-even ^{159,161}Pm: Calling for modified spin-orbit interaction for the neutron-rich region. *Phys. Rev. C* **2021**, *104*, L021303. [CrossRef]
55. Heger, A.; Langanke, K.; Martínez-Pinedo, G.; Woosley, S.E. Presupernova Collapse Models with Improved Weak-Interaction Rates. *Phys. Rev. Lett.* **2001**, *86*, 1678–1681. [CrossRef]
56. Heger, A.; Woosley, S.E.; Martínez-Pinedo, G.; Langanke, K. Presupernova Evolution with Improved Rates for Weak Interactions. *Astrophys. J.* **2001**, *560*, 307. [CrossRef]
57. Misch, G.W.; Ghorui, S.K.; Banerjee, P.; Sun, Y.; Mumpower, M.R. Astromers: Nuclear Isomers in Astrophysics. *Astrophys. J. Suppl. Ser.* **2020**, *252*, 2. [CrossRef]
58. Haxton, W.C.; Henley, E.M. *Symmetries and Fundamental Interactions in Nuclei*; World Scientific: Singapore, 1995.
59. Brown, B.; Wildenthal, B. Experimental and theoretical Gamow-Teller beta-decay observables for the sd-shell nuclei. *At. Data Nucl. Data Tables* **1985**, *33*, 347–404. [CrossRef]
60. Martínez-Pinedo, G.; Poves, A.; Caurier, E.; Zuker, A.P. Effective g_A in the pf shell. *Phys. Rev. C* **1996**, *53*, R2602–R2605. [CrossRef]
61. Märkisch, B.; Mest, H.; Saul, H.; Wang, X.; Abele, H.; Dubbers, D.; Klopf, M.; Petoukhov, A.; Roick, C.; Soldner, T.; et al. Measurement of the Weak Axial-Vector Coupling Constant in the Decay of Free Neutrons Using a Pulsed Cold Neutron Beam. *Phys. Rev. Lett.* **2019**, *122*, 242501. [CrossRef]
62. Nilsson, S.G.; Tsang, C.F.; Sobiczewski, A.; Szymański, Z.; Wycech, S.; Gustafson, C.; Lamm, I.; Möller, P.; Nilsson, B. On the nuclear structure and stability of heavy and superheavy elements. *Nucl. Phys. A* **1969**, *131*, 1–66. [CrossRef]
63. Ring, P.; Schuck, P. *The Nuclear Many-Body Problem*; Springer: Berlin/Heidelberg, Germany, 1980.
64. Varshalovich, D.A.; Moskalev, A.N.; Khersonskii, V.K. *Quantum Theory of Angular Momentum*; World Scientific: Singapore, 1988.
65. Available online: https://www.nndc.bnl.gov (accessed on 9 January 2023).
66. Möller, P.; Sierk, A.; Ichikawa, T.; Sagawa, H. Nuclear ground-state masses and deformations: FRDM(2012). *At. Data Nucl. Data Tables* **2016**, *109–110*, 1–204. [CrossRef]

67. Albers, M.; Zhu, S.; Janssens, R.V.F.; Gellanki, J.; Ragnarsson, I.; Alcorta, M.; Baugher, T.; Bertone, P.F.; Carpenter, M.P.; Chiara, C.J.; et al. Single-particle and collective excitations in ^{63}Ni. *Phys. Rev. C* **2013**, *88*, 054314. [CrossRef]
68. Lederer, C.; Massimi, C.; Altstadt, S.; Andrzejewski, J.; Audouin, L.; Barbagallo, M.; Bécares, V.; Bečvář, F.; Belloni, F.; Berthoumieux, E.; et al. Neutron Capture Cross Section of Unstable ^{63}Ni: Implications for Stellar Nucleosynthesis. *Phys. Rev. Lett.* **2013**, *110*, 022501. [CrossRef] [PubMed]